



Cavitation of Water in Soil

Shengmin Luo, A.M.ASCE¹; William J. Likos, M.ASCE²; and Ning Lu, F.ASCE³

Abstract: Despite increasing awareness that cavitation can be a potential mechanism for drainage of water from soil, comprehensive understanding of its effects on soil water retention (SWR) remains largely elusive. A major obstacle is that pore water pressure is commonly conceptualized and measured as a mean value spatially averaged over the entire representative soil volume, including solid, liquid, and gas phases. Water pressure defined as such does not represent the intermolecular pressure that dictates the cavitation phase change process. Classical theories for predicting water cavitation pressure are critically assessed using recent theory for soil sorptive potential and synthesized to determine cavitation of water in soil. Classical cavitation mechanisms of metastable nucleation that occur on a scale of less than tens of nanometers are unlikely to occur in soil water. Cavitation from entrapped bubbles on rough surfaces of soil particles on a scale of hundreds of nanometers, however, is identified as responsible for soil water cavitation. Specifically, cavitation can occur for soils with pore sizes ranging from 10^{-8} to 10^{-4} m with suction of 0.1-15 MPa but is most prominent in soils with pore sizes from 10^{-7} to 10^{-5} m and suction of 0.1-2.2 MPa (silty soils). A framework for soil water cavitation is proposed, parametrically analyzed, and experimentally validated against measured SWR data obtained using axis translation (AT) and hygrometer-based methods. Results indicate that AT can artificially suppress cavitation that otherwise may be a viable water drainage mechanism for soils in the natural environment. **DOI:** 10.1061/(ASCE)GT.1943-5606.0002598. © 2021 American Society of Civil Engineers.

Author keywords: Soil water cavitation; Homogeneous nucleation; Heterogeneous nucleation; Crevice model; Blake threshold; Soil water retention (SWR); Axis translation (AT); Soil suction.

Introduction

Cavitation is the process of forming vapor bubbles inside or on the boundary of a liquid body under tension. This phase transition phenomenon generally occurs in water when the liquid water pressure falls below saturated vapor pressure, in which case the intermolecular water pressure essentially reaches the tensile strength of liquid water (e.g., Brennen 2013; Lu 2019a). Air—water interfaces with concavity toward the air phase are often found in the pore space of soil under unsaturated conditions (e.g., Hillel 1998), thus indicating a pressure deficit in the liquid phase. This is captured by the so-called negative capillary pressure, with reference to the prevailing atmospheric pressure, and consequently offers the probability for cavitation to occur in soil water, particularly during desaturation processes.

In addition to the capillary pressure, which has a magnitude that can be captured by the Young-Laplace equation (e.g., Tuller et al. 1999; Lu and Likos 2004), soil pore water can also be retained via short-ranged, solid-liquid adsorptive mechanisms (e.g., Derjaguin et al. 1987; Revil and Lu 2013). However, matric potential is often defined in the literature solely by the component of negative capillary pressure (i.e., the difference between water pressure and

Note. This manuscript was submitted on January 19, 2021; approved on April 26, 2021; published online on June 9, 2021. Discussion period open until November 9, 2021; separate discussions must be submitted for individual papers. This paper is part of the *Journal of Geotechnical and Geoenvironmental Engineering*, © ASCE, ISSN 1090-0241.

air pressure), which has led to commonly adopted approaches for characterizing soil water retention (SWR) curves by manipulating the air—water pressure difference and measuring corresponding soil water content. Approaches using pressurized apparatuses such as axis translation (AT) (e.g., Hilf 1956) can prevent cavitation by artificially transferring soil water pressure from below atmospheric pressure to a value equal to or above atmospheric pressure (e.g., von Fay 1985). Whether or not these imposed laboratory conditions can truly reflect SWR under natural conditions, however, is subject to debate. Apparent discrepancies have been observed between AT techniques and other nonpressurized methods such as hygrometer-based [e.g., dew point (DP)] methods (e.g., Chahal and Yong 1965; Baker and Frydman 2009; Bittelli and Flury 2009; Frydman and Baker 2009; Lu 2019b).

While cavitation has been identified as a potential mechanism for water drainage in soil (e.g., Or and Tuller 2002; Toker et al. 2003; Baker and Frydman 2009), current attempts to apply classical theories of acoustic and hydrodynamic cavitation to soil water remain conceptual and qualitative. Classical nucleation theory (CNT) based on the water phase diagram, for example, requires clear understanding of intermolecular pressure from forces that condense water molecules together in the liquid phase. This is different than the common conception of bulk pore water pressure averaged over a representative elementary volume (REV) that includes the larger-scale multiphase soil–water–air system (Nitao and Bear 1996). Cavitation is a macroscopic manifestation of the tensile strength of water, and thus is fundamentally controlled by the intermolecular water pressure rather than the homogenized bulk water pressure commonly adopted in soil mechanics.

Recent advances in defining soil sorptive potential (SSP) quantitatively demonstrate that water pressure near soil particle surfaces (adsorptive water) can be much higher than bulk pore water at the air—water interface (capillary water) (e.g., Mitchell 1962; Lu and Zhang 2019; Zhang and Lu 2020). Both types of soil water can coexist at the same matric potential under local thermodynamic

¹Postdoctoral Fellow, Dept. of Civil and Environmental Engineering, Colorado School of Mines, Golden, CO 80401. ORCID: https://orcid.org/0000-0002-5433-6285. Email: shengminluo@mines.edu

²Professor, Dept. of Civil and Environmental Engineering, Geological Engineering Program, Univ. of Wisconsin–Madison, Madison, WI 53706. Email: likos@wisc.edu

³Professor, Dept. of Civil and Environmental Engineering, Colorado School of Mines, Golden, CO 80401 (corresponding author). ORCID: https://orcid.org/0000-0003-1753-129X. Email: ninglu@mines.edu

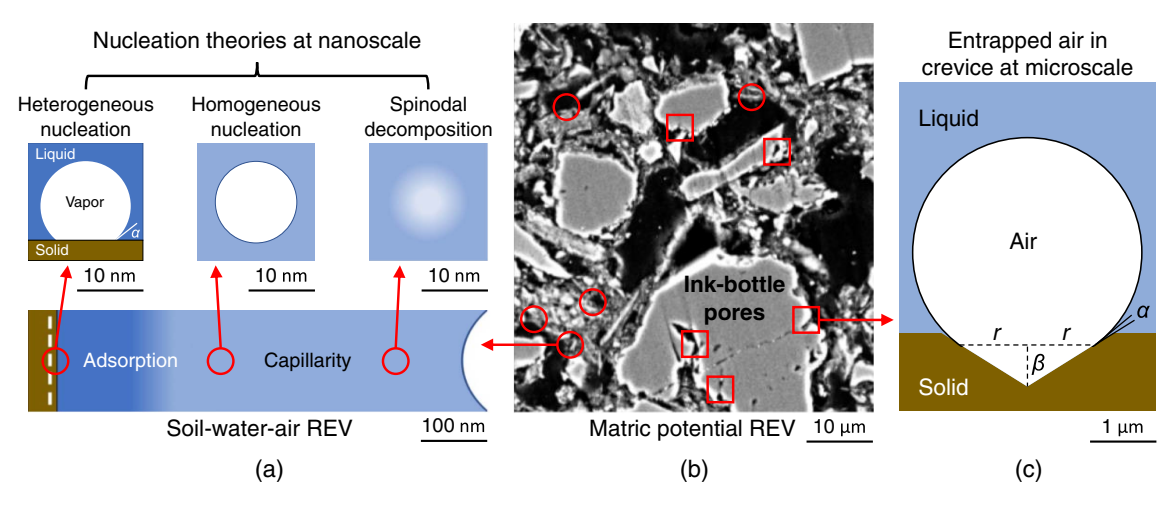


Fig. 1. Potential mechanisms for soil water cavitation: (a) homogeneous nucleation of vapor bubble in capillary water and heterogeneous nucleation at solid–liquid interface, both at the nanometer scale; (b) pore structure of a silty soil (base image from Liu et al. 2016, with permission); and (c) heterogeneous cavitation induced by air trapped on a rough soil particle surface in crevices at the submicrometer to micrometer scale.

equilibrium. Understanding the transition from water retention regimes dominated by capillary mechanisms at relatively high water content and adsorptive mechanisms at relatively low water content remains an active area of research in unsaturated soil mechanics (Akin and Likos 2017, 2020). Because intermolecular adsorptive forces elevate the water pressure locally, which renders adsorbed water less likely to cavitate than capillary water, the occurrence of cavitation can potentially be used to distinguish these two water retention regimes and clarify transitional behavior in soil water retention. A recent generalized SWR curve model (Lu 2016), for example, explicitly integrates the cavitation mechanism into the formulation by imposing a probabilistic cavitation function.

The primary objectives of this study are to critically examine the relevance of classical water cavitation theories to soil pore water and to form a framework for cavitation theory that is more applicable for soil water. Two commonly used nucleation theories are first quantitatively investigated: homogeneous nucleation occurring at a scale less than tens of nanometers within a body of capillary water, and heterogeneous nucleation occurring at a scale less than tens of nanometers at the liquid-solid interface (Fig. 1). The effects of elevated water pressure near soil particle surfaces due to adsorptive forces captured by the SSP are explicitly considered and analyzed, thus representing a departure from CNT. At a scale of greater than hundreds of nanometers (where rough particle surfaces exist), a new simulation framework integrating a crevice model and Blake threshold is presented to examine the cavitation phenomenon in soil under the condition of entrapped gas (Fig. 1). The framework is validated by comparing experimental SWR curve measurements with retention curves calculated from the proposed framework, thus providing quantitative evidence affirming the nonnegligible role that cavitation plays in soil desaturation.

Homogeneous Nucleation in Liquid

Classical Nucleation Theory

First-order phase transition behavior of water under different temperature and pressure conditions has been widely interpreted by using the phase diagram, illustrated as solid curves in Fig. 2(a) (Wagner and Pruß 2002). The pressure of liquid water in soil can drop below the saturated vapor pressure line during desaturation

when the effect of capillarity is introduced, during which the capillary liquid water (see soil–water–air REV in Fig. 1) will transform into vapor. The two phases coexist until all the liquid is turned into vapor. At temperatures lower than the critical temperature, this phase transition takes place under constant pressure (i.e., isobar), depicted by the horizontal section of the isotherm on a pressure–volume (P-V) diagram, as shown by the path B–E in Fig. 2(b) (e.g., Debenedetti 1996; Marinho et al. 2008).

In reality, water can remain in one uniform liquid phase in a metastable state [shaded region in Fig. 2(a) and path B–C in Fig. 2(b)] even under negative pressure (i.e., tension). From the energy perspective, the vapor phase has a lower chemical potential than the liquid phase in metastable water (Debenedetti 1996), which results in a tendency for liquid-to-vapor transition so that a more stable state can be reached. Energy input to the system for nucleation of vapor bubbles (i.e., a stable phase) is generally necessary for phase transition to occur in the metastable liquid. According to the CNT, the total energy change ΔE involved in this nucleation process can be quantified as follows if a common spherical shape is assumed for the vapor bubble (e.g., Caupin and Herbert 2006)

$$\Delta E = \frac{4}{3}\pi R^3 (p_L - p_V) + 4\pi R^2 \sigma \tag{1}$$

where R = radius of the spherical bubble (m); p_L and p_V = liquid water pressure and saturated vapor pressure, respectively (Pa); and σ = surface tension of water (N/m).

Two types of energy change are included in the previous equation: (1) a reduction in volumetric energy due to transformation of water from liquid to vapor, and (2) an increment in interfacial energy corresponding to the formation of new surface (i.e., vapor—liquid interface). As shown in Fig. 2(c), these two competing energy components are both radius dependent, and they act together to form an energy barrier that the metastable liquid water must overcome to move to the state possessing minimum Gibbs free energy (Debenedetti and Reiss 1998; Gunther 2003). In other words, cavitation will not occur unless the bubble nucleus reaches a critical size $R_{\rm crit}$, which may be determined by taking the derivative of Eq. (1) with respect to R and setting it to zero (e.g., Karthika et al. 2016)

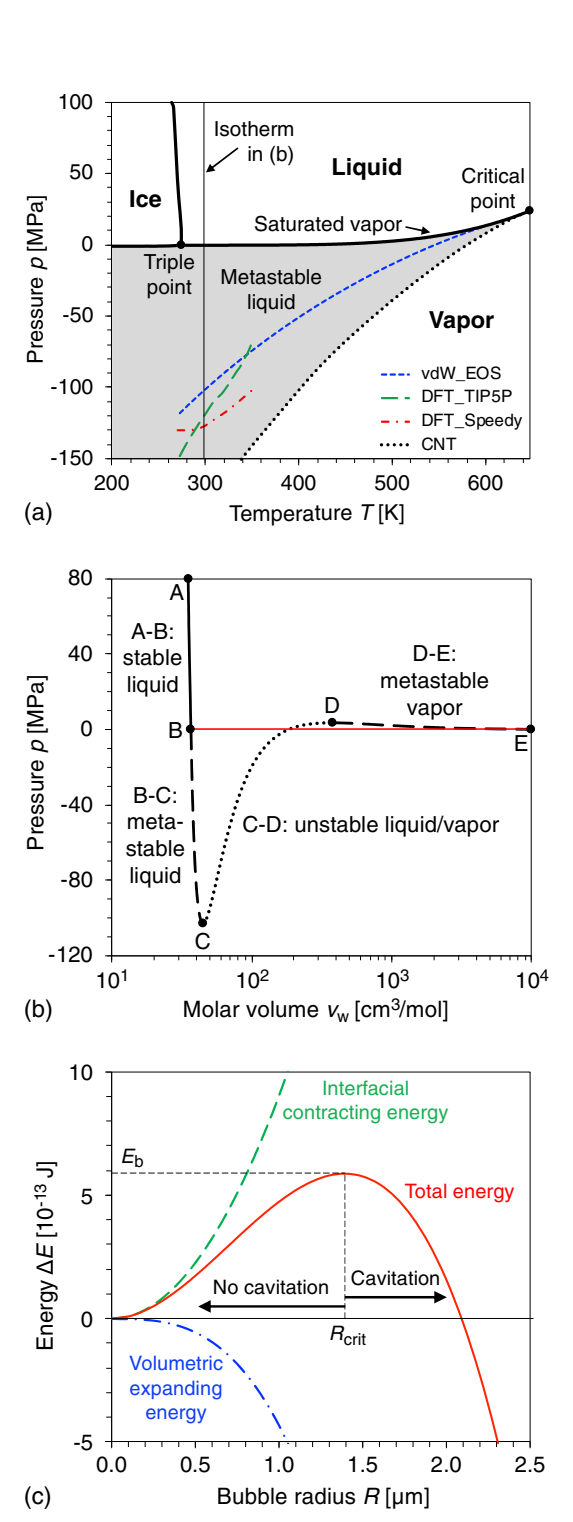


Fig. 2. Thermodynamic conditions for water phase transition: (a) pressure–temperature phase diagram where the shaded region corresponds to the metastable liquid water; (b) van der Waals isotherm obtained at 298.15 K (25°C); and (c) dependence of cavitation energies on the radius of nucleated bubble under water pressure of -100 kPa.

$$R_{\rm crit} = \frac{2\sigma}{p_V - p_L} \tag{2}$$

The corresponding energy barrier E_b (i.e., the minimum reversible work) required to form a critical nucleus can then be obtained by substituting $R_{\rm crit}$ into Eq. (1) as (e.g., Caupin et al. 2012)

$$E_b = \frac{16\pi\sigma^3}{3(p_V - p_L)^2}$$
 (3)

The probability and rate of cavitation occurrence are also related to the energy barrier via the following Boltzmann factor (e.g., Brennen 2013; Maris and Balibar 2000)

$$\exp\left(-\frac{E_b}{k_B T}\right) \tag{4}$$

where k_B = Boltzmann constant of 1.381×10^{-23} (m² · kg · s⁻² · K⁻¹); and T = absolute temperature (K). The probability of cavitation f occurring in an experiment conducted on a volume $V_{\rm exp}$ during a time $\tau_{\rm exp}$ is given by (e.g., Caupin et al. 2012)

$$f = 1 - \exp\left[-\Gamma_0 V_{\exp} \tau_{\exp} \exp\left(-\frac{E_b}{k_B T}\right)\right]$$
 (5)

where Γ_0 = kinetic prefactor ranging between 10^{25} and 10^{27} (cm⁻³·s⁻¹) (Pettersen et al. 1994). Together with Eq. (3), the cavitation pressure $p_{\rm cav}$ can then be predicted by CNT by adopting the pressure at cavitation probability f equal to 0.5 (e.g., Herbert et al. 2006)

$$p_{\text{cav}} = p_V - 1/\sqrt{\frac{3k_B T}{16\pi\sigma^3} \ln\left(\frac{\Gamma_0 V \tau}{\ln 2}\right)}$$
 (6)

where $\Gamma_0 V \tau$ can be treated as a constant with limiting effect on $p_{\rm cav}$; and a typical value of 10^{19} is suggested for acoustic cavitation in water (e.g., Caupin et al. 2012).

Spinodal Limit

A physical limit on negative pressure should exist even for pure, deaired water. This limit is known as the spinodal limit and it separates the metastable region from the unstable region. When the liquid pressure drops below the spinodal limit, the energy barrier required by nucleation of vapor bubbles disappears such that phase transition occurs spontaneously (e.g., Shamsundar and Lienhard 1993), referred to as spinodal decomposition (e.g., Favvas and Mitropoulos 2008; Lienhard et al. 1986).

The water isotherms on the P-V diagram [Fig. 2(b)] can be described by the well-known van der Waals equation of state (EOS)

$$p = \frac{\bar{R}T}{v_w - b} - \frac{a}{v_w^2} \tag{7}$$

where p = pressure (Pa); and v_w = molar volume of water (either liquid or vapor) (m³/mol); \bar{R} = universal gas constant of 8.3145 (J·mol⁻¹·K⁻¹); and a and b = two constants respectively corresponding to long-range attractions and short-range repulsions between molecules, and for water their values are 0.5537 (Pa·m⁶·mol⁻²) and 3.049 × 10⁻⁵ (m³/mol) (roughly the volume occupied by the molecules) (Silbey et al. 2004).

A water isotherm for 25°C is calculated by using the preceding van der Waals EOS (vdW_EOS) and shown in Fig. 2(b). Point B represents the saturated vapor pressure, and point C is the spinodal limit where the thermodynamic stability criteria are violated (Debenedetti 1996). Therefore, the vapor phase is more stable than the liquid phase along the path B–C, and phase transition from liquid to vapor initiates (i.e., vertically toward the path B–E) if the nucleus of a vapor bubble is present in the liquid. A spinodal limit of –102.8 MPa is obtained for 25°C based on the isotherm of water (point C), which in fact is a much higher pressure limit than that predicted by the CNT at the same temperature.

This apparent contradiction in cavitation pressures predicted by two theories is for two reasons. First, the CNT ignores the thickness of the vapor bubble wall in the calculation of Eq. (1) and thus assumes an abrupt change of density across the vapor-liquid interface. This so-called thin wall approximation (TWA) may not be sound when the nucleated bubble size is at the same order of magnitude as the interfacial width. Second, although more complicated EOS can be considered for more accurate predictions, the van der Waals EOS actually provides a fairly good estimation of the tensile strength of pure liquid water (Groß and Pelz 2017), while this physical limit is also neglected by the CNT. Improvements can be achieved by the combination of density functional theory (DFT) and better EOS. Additional results from the literature (e.g., Caupin 2005; Caupin and Herbert 2006; Herbert et al. 2006; Maruyama et al. 2018) are plotted in Fig. 2(a) for comparison, including DFT with speedy EOS (DFT_Speedy) and DFT with EOS calculated by molecular dynamics simulations using the five-site transferable interaction potential (DFT_TIP5P). It is unsurprising to observe that the CNT always overestimates the cavitation pressure at a given temperature.

Suppression of Homogeneous Nucleation by Soil Sorptive Potential

The addition of a soil solid phase further complicates the matter. The importance of using local intermolecular water pressure rather than bulk pore water pressure for the study of multiphase problems in soil (e.g., cavitation and freezing) has been recognized recently by considering the concept of soil sorptive potential (Lu and Zhang 2019). Here, local water pressure p_w can be expressed as a function of water content w and the statistical distance x from the location of interest to an adjacent particle surface (Lu and Zhang 2019)

$$p_w(x, w) = \psi_m(w) - \psi_{\text{sorp}}(x) + p_a$$
 (8)

where ψ_m = matric potential; and ψ_{sorp} = SSP whose magnitude (Pa) highly depends on x (nm); and p_a = air pressure (Pa). The water pressure (Pa) can be further divided into capillary ($p_{w\text{-cap}}$) and sorptive ($p_{w\text{-sorp}}$) components according to their mechanisms of water retention (Lu 2020). SSP is the summation of four components corresponding to the four intrinsic intermolecular forces in soil, which include the van der Waals component, electrical component, osmotic component, and hydration component. Further detailed discussion about the SSP and its four components can be found in the literature (Lu and Zhang 2019).

For a fully saturated condition, ψ_m is zero and the capillary component of water pressure $(p_{w-\text{cap}}-p_a)$ vanishes. Based on Eq. (8), the water pressure at a specific location of the pore space is thus 100% converted, but with a negative sign, from the SSP determined at the same place. Fig. 3(a) shows profiles of SSP and water pressure in a parallel-plate pore that is 20 nm in size. Because the van der Waals component in SSP is the most common mechanism that alters the magnitude of water pressure near the soil particle surface, two different values of Hamaker constant, -3.1×10^{-20} and $-2.2 \times 10^{-20} J$ (denoted in the plot as vdW-1 and vdW-2, respectively), are considered to cover various types of clay minerals (Lu et al. 2008). The theoretical calculation for a saturated condition indicates that the local pore water pressure at 0.2 nm to the soil particle surface can be as high as 10⁶ kPa [Total SSP-1 in Fig. 3(a)]. However, only the water pressure within three layers of water molecules (about 1 nm) is sensitive to the change in Hamaker constant (Lu and Zhang 2019), and a 41% reduction is found for the highest water pressure when switching from vdW-1 to vdW-2.

To consider the possibility of soil water cavitation under unsaturated condition (assuming pure and deaired water), a semicircular

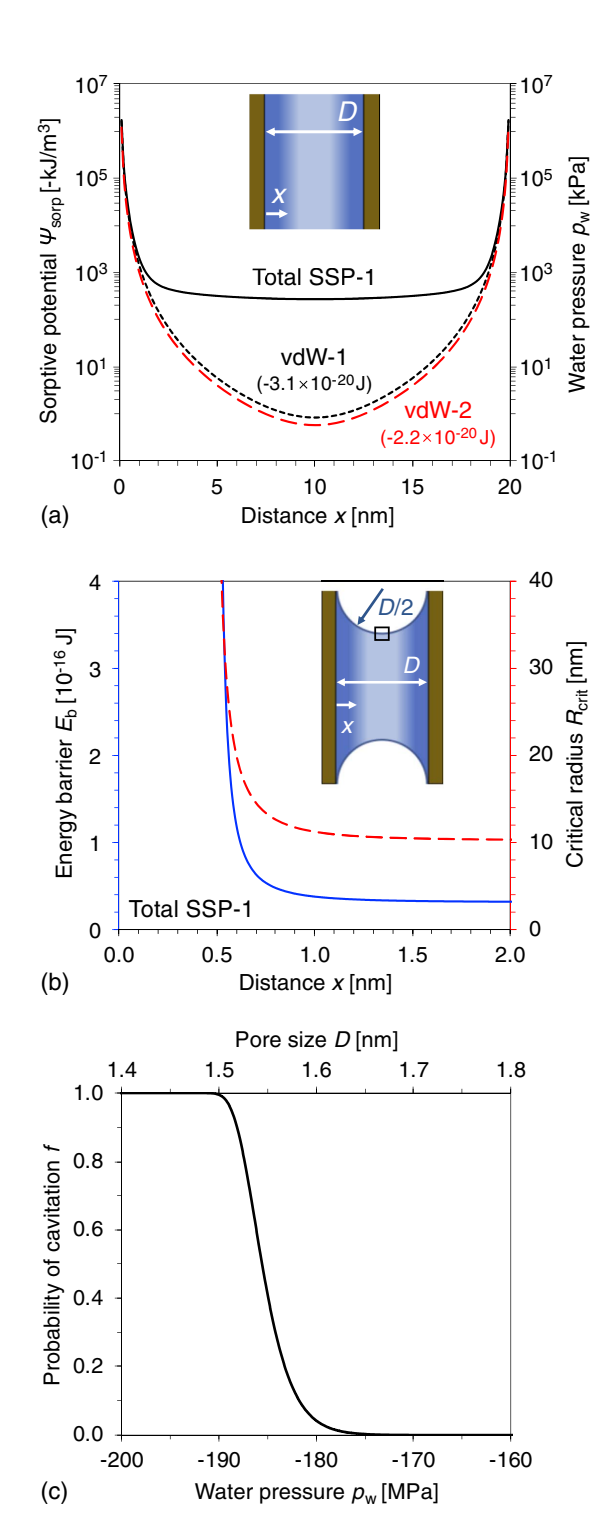


Fig. 3. Pressure and energy barrier distributions in soil pores: importance of SSP in (a) pressure and (b) energy barriers; and (c) probability of cavitation under different water pressures.

interface between air and liquid is introduced to the previous saturated pore configuration [inset in Fig. 3(b)]. The capillary potential ψ_{cap} at the location next to the air—water interface (indicated by the square box) can be determined by the Young-Laplace equation (e.g., Lu and Likos 2004)

$$\psi_{\rm cap} = -\frac{4\sigma}{D} \tag{9}$$

where D = separation distance between two plates and is equal to 2×10^{-8} m (20 nm). A capillary water pressure of -14,400 kPa (-14.4 MPa) is calculated at the midplane (x = D/2), and the matric potential is then determined as

$$\psi_m(w) = \psi_{\text{cap}} + \psi_{\text{sorp}}(x = D/2) \tag{10}$$

To satisfy the local thermodynamic energy equilibrium, the matric potential should be the same everywhere inside the pore space, and the water pressures at any other locations can be obtained by using Eq. (8). As such, the profiles of the energy barrier and critical radius required for homogeneous nucleation of vapor bubble in an unsaturated pore can be characterized using Eqs. (2) and (3).

The probability distribution of cavitation obtained in terms of Eqs. (3)–(5) at different water pressures is presented in Fig. 3(c) for 25°C. Results show that the possibility of cavitation quickly turns from impossible to inevitable within a narrow range of pressure change (decrease from -180 to -190 MPa). Based on the probability function of homogeneous nucleation [Fig. 3(c)], cavitation via nucleation of a vapor bubble in the capillary water is impossible in the pore configuration considered in Fig. 3(b) (-14.4 MPa capillary pressure). Moreover, because the negative water pressure is the result of the curved air-water interface at the pore entrance, the cavitation pressure predicted at around -100 MPa only has a chance of occurring in nanopores [D < 2 nm as provided by Fig. 3(c)]. Results in Fig. 3(b), however, suggest that due to the increasing water pressure caused by the SSP, both E_b and R_{crit} increase drastically when approaching the particle surface (x < 0.7 nm). In such space (the nanopore), the SSP is the dominant mechanism of soil-water interactions over capillarity, which renders cavitation induced by homogeneous nucleation even more unlikely to happen.

Heterogeneous Nucleation Near a Soil Particle Surface

Effect of Surface Wettability

In practice and as shown previously, homogeneous nucleation (e.g., > -100 MPa) is difficult to achieve by laboratory experiments because the bubbles generally tend to nucleate at the wall of the container when the metastable liquid is in contact with a solid surface. For instance, a wide variety of cavitation pressures has been reported in different studies using various experimental techniques: -7 MPa for evaporation in silica nanochannels (Duan et al. 2012), -16 MPa for acoustic cavitation in stainless steel cell (Greenspan and Tschiegg 1967), -28 MPa for centrifugation in Pyrex capillaries (Briggs 1950), and -140 MPa for quartz inclusions (Zheng et al. 1991). A more comprehensive summary can be found in Caupin and Herbert (2006).

When purified water is stored in a solid container, vapor–solid and liquid–solid interfaces form in addition to the vapor–liquid interface and hence the wettability of the surface plays an important role during this process. The energy barrier $E_{b\text{-het}}$ for heterogeneous nucleation on a flat and smooth surface (Fig. 1) can be formulated as (e.g., Belova et al. 2010; Giacomello and Roth 2020)

$$E_{b\text{-het}} = \frac{16\pi\sigma^3}{3(p_V - p_L)^2} \cdot g(\alpha) \tag{11}$$

This expression is similar to that of CNT given as Eq. (3), but includes an additional correction term $g(\alpha)$ (e.g., Belova et al. 2011; Blander and Katz 1975)

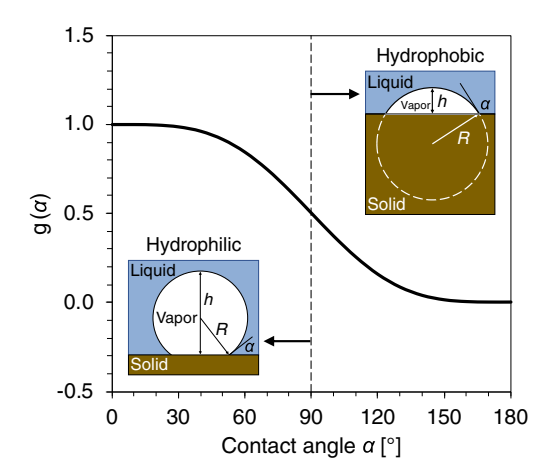


Fig. 4. Geometry correction function for the energy barrier required to form a critical bubble nucleus at the particle surface.

$$g(\alpha) = \frac{2 + 3\cos\alpha - \cos^3\alpha}{4} \tag{12}$$

where α = equilibrium contact angle of water on the surface. A plot of the function $g(\alpha)$ is displayed in Fig. 4, showing that the value of function $g(\alpha)$ ranges from 1 to 0 as the surface wetting property switches from hydrophilic to hydrophobic. As also shown by the two insets in Fig. 4, a well-wetted surface has a comparable energy barrier to that for homogeneous nucleation, while the presence of a hydrophobic surface significantly reduces, or even eliminates, the energy used for bubble nucleation. For example, a 37% reduction is found for the energy barrier if α increases from 20° to 80°. Moreover, the maximum height h of the bubble nucleated above the solid surface (insets in Fig. 4) also depends on the contact angle of the solid surface, which is determined as follows by considering the geometric relationship shown in Fig. 4

$$h = \frac{2\sigma}{(p_V - p_W)} (1 + \cos \alpha) \tag{13}$$

where p_w = water pressure near the particle surface, and for simplicity is assumed to be spatially uniform in the following calculations.

Suppression of Heterogeneous Nucleation by SSP

Fig. 5 presents the energy barrier $E_{b-{\rm het}}$ and bubble height hcalculated for heterogeneous nucleation on surfaces with varying contact angles. Two different pore water pressures, -10 and -100 MPa, are considered. For the same pressure, the $E_{b\text{-het}}$ and h obtained from surface with α < 50° are about three and two orders of magnitude higher, respectively, than those obtained from $\alpha > 160^{\circ}$. According to Fig. 4, $E_{b\text{-het}}$ can theoretically become zero when α approaches 180°, no matter which water pressure is encountered. Consequently, the probability of cavitation f triggered by heterogeneous nucleation on surfaces with different contact angles can also be calculated by Eq. (5), and the cavitation is assumed to certainly occur while f is greater than 0.5. The results shown in Fig. 5(c) demonstrate that the tensile strength of water can be reduced significantly by the presence of a hydrophobic surface (Factorovich et al. 2014). For instance, when the water pressure is relatively high, such as -10 MPa [around the same order of magnitude as that considered Fig. 3(b)], cavitation only appears on the surface with superhydrophobicity ($\alpha > 160^{\circ}$), but for most soil surfaces, the contact angle is less than 60°, meaning that

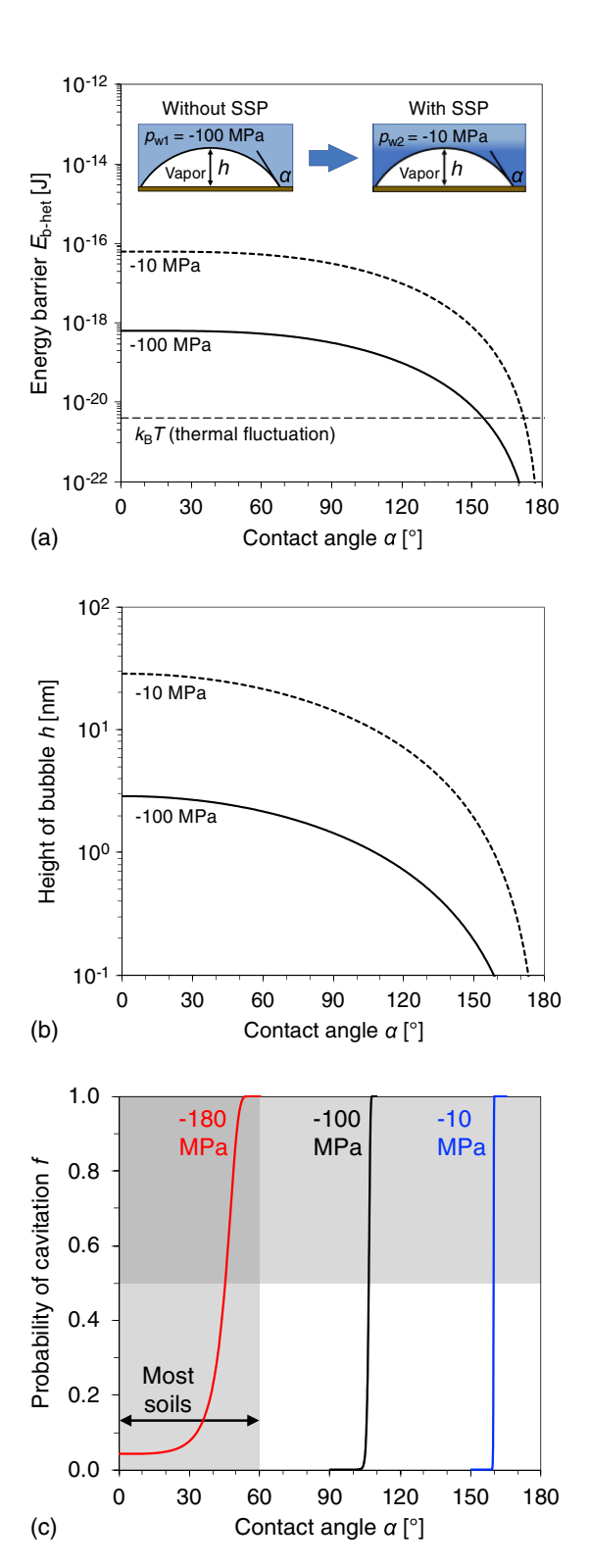


Fig. 5. Required minimum work and probability for heterogeneous nucleation: (a) height of nucleated bubble; (b) calculated as a function of contact angle at two pore water pressures to account for the effect of SSP; and (c) probability under different conditions.

a water pressure close to the cavitation pressure predicted by CNT [e.g., -180 MPa in Fig. 5(c)] is required for the thermal fluctuation of water molecules to overcome the barrier of heterogeneous nucleation.

However, as discussed in the previous section, the SSP will increase the local water pressure near the soil surface, and the bubble height exactly falls within the range (10–20 nm) that the SSP plays a significant role. Assuming the water pressure increases from -100 to -10 MPa because of the SSP, it is obvious to observe that $E_{b\text{-het}}$ and h at any contact angle increase 100 and 10 times (Fig. 5), respectively, rendering the cavitation at room temperature unlikely to take place even on the hydrophobic surface [e.g., α from 90° to 160° in Fig. 5(c)]. Therefore, the strength of SSP will also suppress the heterogeneous nucleation of the vapor bubble on the soil particle surface to different extents. As mentioned previously, the soil particle surfaces are generally hydrophilic (Zheng and Zaoui 2017), which, combined with the effect of SSP, causes the appearance of heterogeneous cavitation on the soil surface even rarer.

Framework for Entrapped Gas Nucleation in Soil

Crevices produced by rough and uneven surfaces in soil are common at a scale greater than hundreds of nanometers (e.g., silt particles in Fig. 1) and could provide favorable locations to entrap air. These sites can later serve as the initial bubble nuclei for cavitation during desaturation. A crevice model and bubble stability criteria can be considered to propose a calculation framework to simulate the process of bubble growth and to quantitatively determine the cavitation pressure in soil at different pore sizes. Because the effect of a preexisting nucleus is insignificant when the size of the crevice is relatively small, as discussed in the following sections, only capillary water retained in the large-enough pores is considered by the proposed framework.

Crevice Model for Bubble Formation

The cavitation pressure in soil under natural conditions can be significantly lower than that predicted using the classical CNT due to the presence of impurities, among which entrapped gas plays the most prominent role for promoting cavitation (Chahal and Yong 1965). A crevice model with an idealized geometry (Fig. 6) demonstrates how the preexisting gas is stabilized as a nucleus and evolves into a bubble as a seed for cavitation (Atchley and Prosperetti 1989). Here, a conical shape is considered with geometry described using half apex angle β and a radius of the base of cone r. Figs. 6(a and b) show two possible configurations for the air-water interface during desaturation. Theoretically speaking, the interface can also be convex toward the air when stable (Or and Tuller 2003), but this is rarely the case if positive hydrostatic pressure is not taken into account. The initial points of contact where the air-water interface meets the solid surface are assumed to be slightly lower than the flat surface outside the crevice mouth, so that the contact angle α is determined as the angle between the side wall of the crevice and interface.

Because desaturation of soil continuously lowers the bulk water pressure in the pore space, the air trapped inside the crevice gradually evolves into a spherical bubble and eventually detaches from the wall of the crevice [Fig. 6(c)]. The interfacial motion is achieved quasi-statically through a sequence of equilibrium configurations, with negligible effects of viscosity and inertia. A mechanically stable bubble's state of equilibrium can be formulated as (Atchley 1989; Or and Tuller 2003)

$$p_G(R) + p_V = p_L + \frac{2\sigma}{R} \tag{14}$$

where the air pressure inside the bubble consists of saturated vapor pressure p_V (Pa) and partial gas pressure p_G (Pa), which, as discussed subsequently, depends on the radius of bubble R (m); p_L = liquid water pressure (Pa); and σ = surface tension of water at a

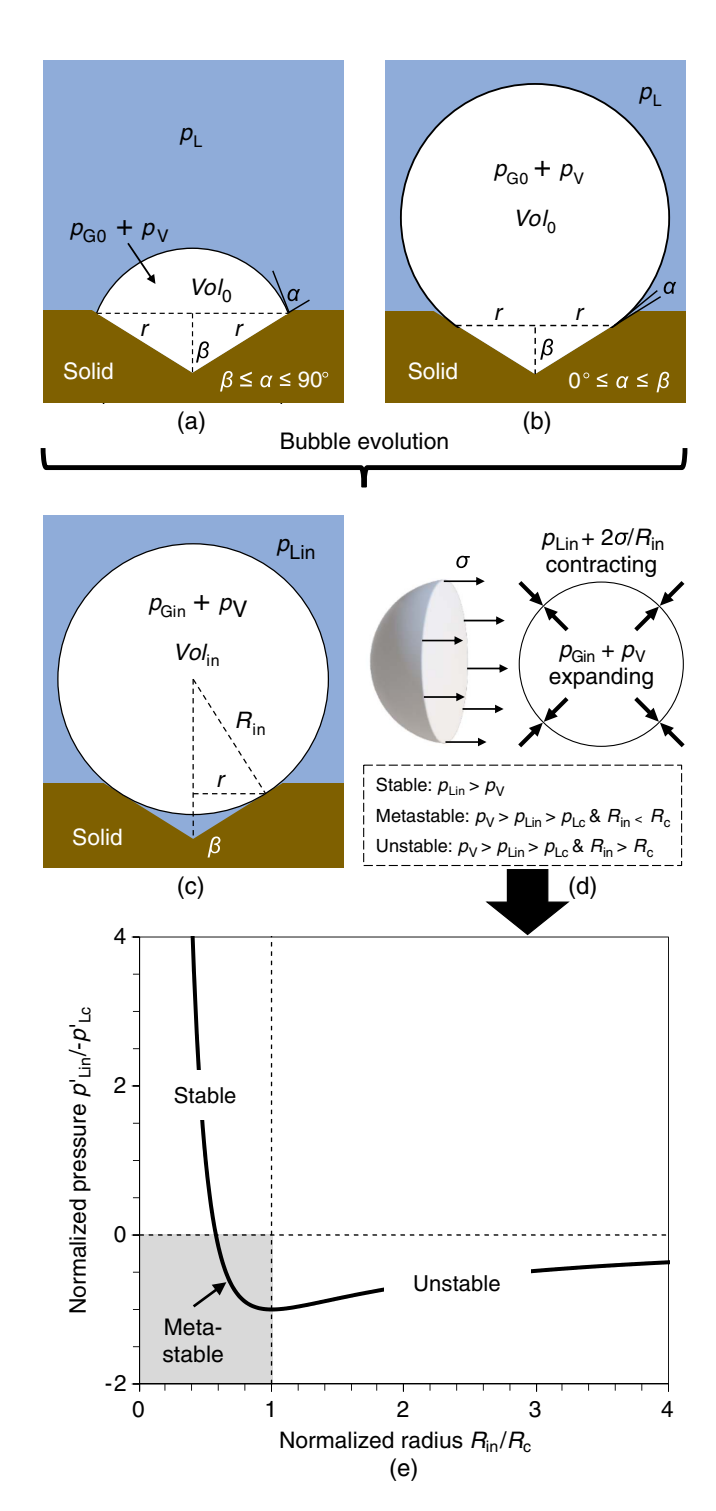


Fig. 6. Parametric analysis for the effects of preexisting gas nucleus on cavitation in soil: entrapped gas bubble stabilized via the conditions of (a) $\beta \le \alpha \le 90^\circ$; and (b) $0^\circ \le \alpha \le \beta$; (c) a spherical free bubble detached from the particle surface due to the reduction in water pressure; (d and e) criteria for mechanical stability of the initial free bubble.

given temperature (N/m). Generally, the left- and right-hand sides of the preceding equation represent the expanding and contracting pressures, respectively [Fig. 6(d)]. If the spherical bubble depicted in Fig. 6(c) is in a form of mechanical equilibrium, these two types of pressure should balance each other in such a way that Eq. (14) is satisfied [Fig. 6(d)].

Assumptions are necessary to determine the parameters for the initial state of the free-floating bubble and to make the bubble

formation process mathematically tractable. First, it is assumed that the points of contact do not change with the motion of the air—water interface and remain fixed at the crevice mouth [Fig. 6(c)]. Thus, the initial bubble radius $R_{\rm in}$ and volume ${\rm Vol}_{\rm in}$ at the moment of detachment can be calculated as

$$R_{\rm in} = \frac{r}{\cos \beta} \tag{15}$$

$$Vol_{in} = \frac{4}{3}\pi R_{in}^3 \tag{16}$$

Second, the bubble evolves isothermally and thus the saturated vapor pressure is a constant (e.g., 3.2 kPa at 25°C). Third, the gas obeys the ideal gas law and no gas diffusion occurs during the process such that the initial partial gas pressure p_{Gin} is found by Boyle's law

$$p_{Gin} = p_{G0} \frac{\text{Vol}_0}{\text{Vol}_{in}} \tag{17}$$

where p_{G0} and Vol₀ = partial gas pressure (Pa) and volume (m³) of air inside the crevice, respectively. The term p_{G0} is 98.1 kPa at 25°C if assuming atmospheric pressure (i.e., 101.3 kPa) for the trapped air. The space occupied by the air can be treated as a combination of two parts, a segment of sphere and a complete cone, whose total volume is calculated by Atchley and Prosperetti (1989)

$$Vol_0 = \frac{1}{3}\pi r^3(\cot\beta + \eta)$$
 (18)

where η = factor that only depends on α and β angles

$$\eta = \frac{2 - [2 + \cos^2(\alpha - \beta)\sin(\alpha - \beta)]}{|\cos^3(\alpha - \beta)|} \tag{19}$$

Finally, the initial liquid pressure p_{Lin} is attainable by rewriting Eq. (14) to

$$p_{Lin} = p_{Gin} + p_V - \frac{2\sigma}{R_{in}}$$
 (20)

Blake Threshold

Preexisting air bubbles that are originally stable in the water can grow with decreasing liquid pressure. The equivalence between expanding and contracting components of bubble [Fig. 6(d)] can no longer be maintained once the surrounding liquid pressure is reduced lower than a certain limit. In this case, the Blake threshold refers to the additional tensile pressure required to cause the indefinite growth of the bubble and is given by $p_B = p_{Lin} - p_{Lc}$, where p_{Lin} is the initial liquid pressure and p_{Lc} denotes the critical liquid pressure (i.e., pressure limit for cavitation).

The general Blake threshold (i.e., the difference in liquid pressure) is helpful when the acoustic cavitation is of interest (Blake 1949), but the critical pressure itself is more important for the understanding of cavitation behavior in soil. According to the stabilization criterion given by Eq. (14), Fig. 6(d) classifies the mechanical stability of a bubble into the following three different states (Atchley 1989)

Stable equilibrium: $p_{Lin} > p_V$

Metastable equilibrium: $p_V > p_{Lin} > p_{Lc}$ and $R_{in} < R_c$

Unstable equilibrium: $p_V > p_{Lin} > p_{Lc}$ and $R_{in} > R_c$ (21)

Here, the cavitation pressure p_{Lc} is crucial for the previous inequalities and can be found by

$$p_{Lc} = p_V - \frac{2(p_{Lin} - p_V)}{3} X_{in} \sqrt{\frac{X_{in}}{3(1 + X_{in})}}$$
 (22)

where

$$X_{\rm in} = \frac{2\sigma}{(p_{\rm Lin} - p_{\rm V})R_{\rm in}} \tag{23}$$

The corresponding bubble radius under the critical pressure for cavitation is calculated as

$$R_c = -\frac{4\sigma}{3(p_{Lc} - p_V)}\tag{24}$$

Following Eqs. (22) and (23), p_{Lc} can be determined as long as the parameters of the initial state of bubble are known. This pressure provides the lower limit of liquid pressure beyond which the bubble growth becomes unstable and would persist even if the decline of the liquid pressure were to stop (i.e., cavitation). Surface tension is assumed to be independent of the bubble radius and is

treated as a constant in the previous calculations for a certain temperature.

Metastable State of Bubble Nucleation in Soil

Based on the preceding discussion, a unique cavitation pressure can be determined in terms of a predefined crevice geometry and surface wettability using the adopted crevice model and Blake threshold. Therefore, a parametric study was conducted in this work for investigating the cavitation behavior of soil water, and the proposed framework is demonstrated by a flowchart in Fig. 7. Three parameters are involved in this process: contact angle α , half apex angle β , and radius of crevice mouth r. Parameter α was selected between 0° and 60° to cover the most common situations of soil surfaces [e.g., Fig. 5(c)], while β was varied between 1° and 89°. Both variables were sampled at 1° intervals (i.e., 61 and 89 increments for α and β , respectively). The r values ranging from 0.01 to 50 μ m were sampled every 0.01 μ m (i.e., 5,000 increments). A total of 27.145,000 (i.e., $61 \times 89 \times 5,000$) combinations of these three variables can then be found. The probability of occurrence for each of the α - β -r configurations is assumed equal.

A pair of R_c and p_{Lc} was calculated for a critical state bubble produced from each increment of α - β -r configuration based on

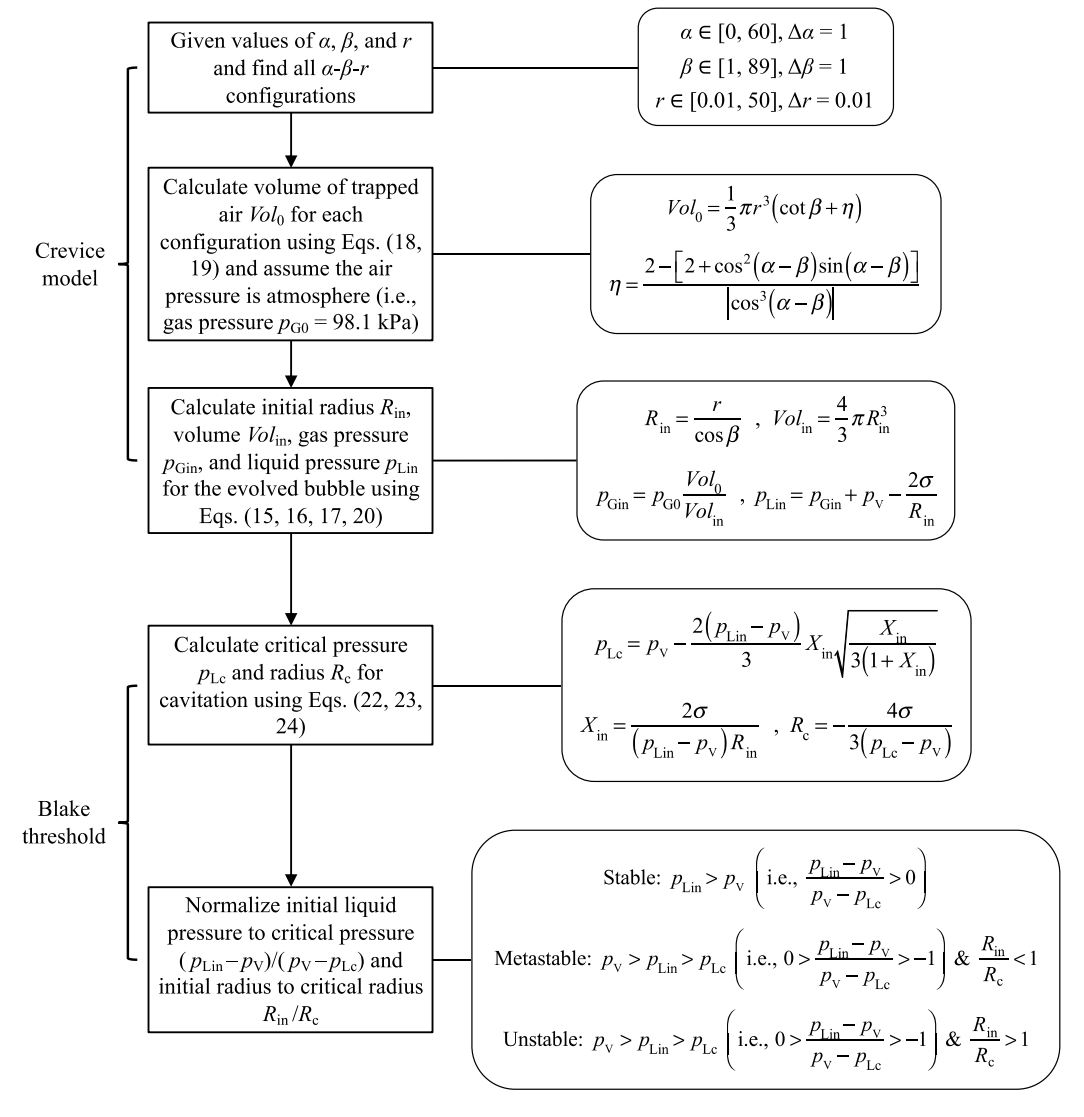


Fig. 7. Proposed framework for characterization of soil water cavitation.

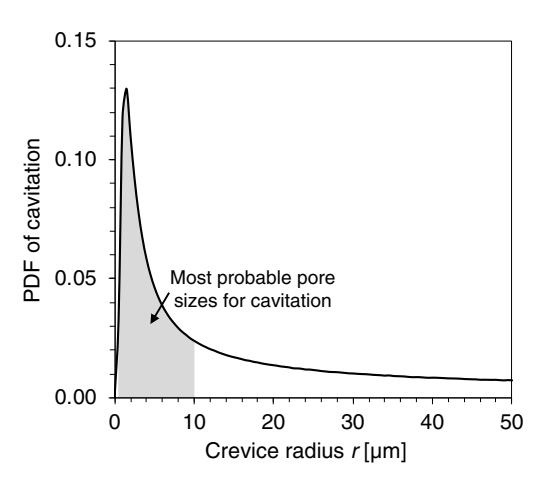


Fig. 8. PDF of cavitation events, indicating that the cavitation in soil caused by entrapped gas generally takes place in micrometer to submicrometer pores.

five steps described in the flowchart (Fig. 7). Fig. 6(e) presents the results obtained from the parametric study, showing equilibrium water pressure as a function of bubble radius. The pressure values are attained by normalizing the difference between initial liquid pressure and vapor pressure $(p'_{Lin} = p_{Lin} - p_V)$ to the difference between vapor pressure and critical liquid pressure $(-p'_{Lc} =$ $p_V - p_{Lc}$). The initial radius of each scatter point is also normalized to the critical radius. The entire plot is divided into three regions according to the previous classification of equilibrium state of bubble. The initial radius in Regions 1 and 2 is at the same order of magnitude as the critical radius, so the r of data points in these two regions can be used to approximate the pore radius in soil (or at least set the lower bound). In this work, only the results belonging to Region 2, which contains 1,777,473 configurations, will be considered in the subsequent data analysis for the following two reasons. First, Region 1 corresponds to the stable equilibrium under positive water pressure and the results therein are mainly calculated from the configurations with relatively large r values (e.g., r > r1 μ m). However, this usually is not the case in desaturating soils due to the capillary effect, as long as the positive hydrostatic pressure is assumed to be negligible. Second, Region 3 corresponds to the unstable equilibrium and indicates that the initial bubble is already larger in size than that of the critical state. This suggests that the assumption of mechanical equilibrium based on Eq. (14) for the initial free bubble is violated because any infinitesimal change in the bubble radius caused by disturbance can result in uncontrollable bubble growth.

As previously mentioned, each of the 1,777,473 α - β -r configurations can determine a critical water pressure at which soil water starts to cavitate. The configurations with the same r value are then assigned to the same group, followed by the generation of a probability density function (PDF) in terms of the pore size, as shown in Fig. 8. A direct observation from this plot is that a sharp peak occurs at approximate $r = 1 \mu \text{m}$ (i.e., 10^{-6} m), and most configurations concentrate within the range of pore size between 0.3 and 10 μ m. This demonstrates that soil water cavitation triggered by preexisting gas entrapped in the crevice usually occurs when the pore space is large enough (e.g., $>0.3 \mu m$) for the bubble to grow beyond its critical size. Moreover, such gas-promoted cavitation does not appear in very large pores (several tens of micrometers), so this type of cavitation should be expected within a certain range of pore size (0.3–10 μ m), and the most suitable candidate would be the silty soils.

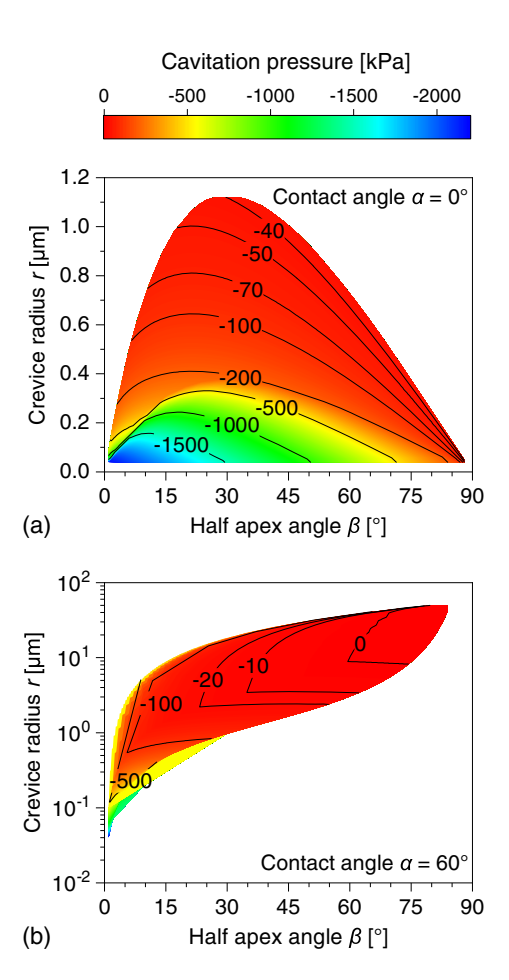


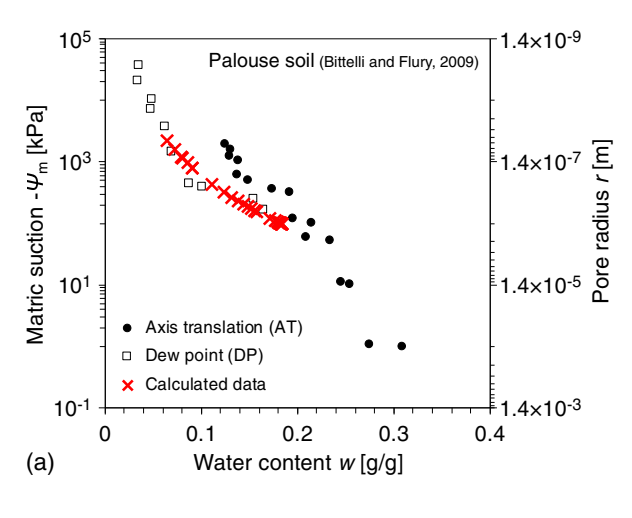
Fig. 9. Cavitation pressure in metastable regimes determined at contact angles of (a) 0°; and (b) 60° in soil.

Fig. 9 further exemplifies the results by contour plots of cavitation pressure generated for the selected contact angles of 0° and 60°. According to Figs. 9(a and b), a wide range of cavitation pressure is obtained from as low as -2,100 kPa to as high as 3 kPa, and an overall increasing trend is observed in cavitation pressure with the increasing α . Generally speaking, -500 to 0 kPa is the most probable range for cavitation pressure in soil, but bubbles trapped in the submicrometer-sized and narrow (i.e., both r and β are small) pores will cavitate at much lower pressures [e. g., the region enclosed below -1,500 kPa contour line in Fig. 9 (a)] and vice versa. In addition, when the pore size is relatively smaller, results do not exist if both α and β are large [e.g., Fig. 9 (b)]. Additional significance of Fig. 9 is that, if the pore size distribution (PSD) or the distribution of crevice geometry is known for a given type of soil, the cavitation pressure can be easily determined according to these contour plots.

Validation of Water Cavitation in Soil

Predicting Soil Water Retention Curve

Based on the preceding analysis, for silty soils with dominant pore sizes between 10^{-7} and 10^{-5} m, cavitation can play a significant role in soil water drainage and hence is important for accurately measuring the SWR curve. Attention has been given to the discrepancy in SWR measurements that were collected for silty soils using both AT and DP methods (Bittelli and Flury 2009). As shown in Fig. 10(a), the water contents of a silty soil measured by AT start to



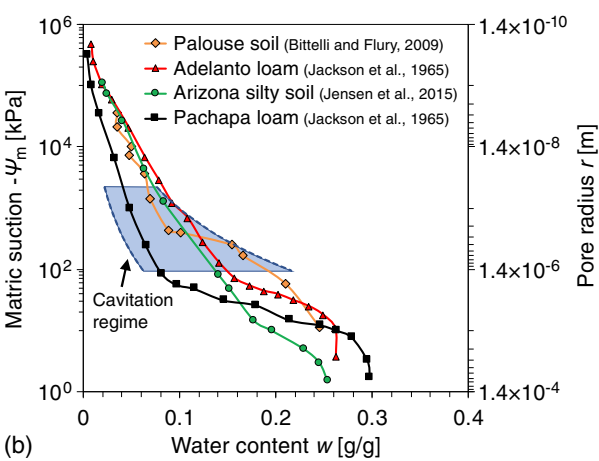


Fig. 10. (a) Cavitation suppression by AT while measuring SWR curve; and (b) further comparison between the experimental SWR measurements in the literature and the simulation results obtained in this study by using a common range of specific surface area (SSA).

deviate from those measured by DP when the matric suction is greater than roughly 100 kPa, and this disagreement becomes even larger as the matric suction further increases to around 2,000 kPa (2 MPa). For such reason, the AT has been considered to provide misleading SWR measurements for silty soils because it overlooks the significance of cavitation of capillary water by raising the pore water pressure during testing (Baker and Frydman 2009; Lu 2019b).

Predicting the Likely Cavitation Regime in Soil Water Retention

A representative cavitation pressure can be obtained for each pore size by averaging the results determined from the configurations with the same r value, and accordingly the SWR data for a given silty soil can be calculated by using the framework presented in this study. As shown in Fig. 8, cavitation mainly occurs in silty soils with micrometer to submicrometer pores $(10^{-5} \text{ m} > r > 10^{-7} \text{ m})$, where capillarity dominates and the contribution of SSP is negligible at these scales. Therefore, the adsorption mechanism in soil is less prominent and the matric potential ψ_m can be approximated by only considering the capillary component, i.e., the difference between pore water pressure p_w and pore air pressure p_a (assuming atmospheric pressure)

$$\psi_m(w) = p_w(w) - p_a \tag{25}$$

where p_w is replaced by the representative cavitation pressure p_{cav} determined for each r. Once cavitation has taken place in a pore space, capillary water turns to vapor and only liquid water remains in the form of adsorptive films. The gravimetric water content can be determined by using the following scaling relationship (Tuller and Or 2005; Zhang and Lu 2020)

$$w = h \times SSA \times \rho_w^{\text{ave}} \tag{26}$$

where SSA = soil specific surface area (m^2/g); ρ_w^{ave} = average density of water film (g/cm^3); and h = equilibrium film thickness. If considering van der Waals force as the governing component of adsorption on soil particle surface (Lu and Zhang 2019), h can be expressed as a simple function of matric potential (Iwamatsu and Horii 1996)

$$h = \left(\frac{A_H}{6\pi\psi_m}\right)^{1/3} \tag{27}$$

where A_H = Hamaker constant (J). Therefore, the SWR data for a silty soil can be calculated by assigning $60 \text{ m}^2/\text{g}$ for SSA, $-3.1 \times 10^{-20} \text{ J}$ for A_H , and 1.2 g/cm^3 for ρ_w^{ave} . The Hamaker constant for fine-grained soils only varies within a small range and here its value was selected to be representative of kaolinite particles (Lu et al. 2008). A higher water density is intentionally assumed here, primarily because water density in the adsorptive film can be as high as 1.7 g/cm^3 because of the SSP and will decrease nonlinearly to the density of free water (or even lower under tension) with the increasing distance from the particle surface (Zhang and Lu 2018, 2020).

With the calculated matric potential, matric suction is then defined as the negative of matric potential $-\psi_m$ (Lu and Khorshidi 2015). The matric suction calculated from this work falls within the range of 100-2,200 kPa, and only part of the SWR results are plotted in Fig. 10(a) together with the experimental measurements for comparison. It can be observed that the calculated data follow closely with the DP measurements, indicating that cavitation is an important mechanism controlling the SWR behavior, especially for silty soils. Therefore, the SWR data obtained from AT may not be representative for silty soils during the natural desaturation process because it indeed suppresses the cavitation of capillary water during testing. Additional evidence of soil water cavitation is provided in Fig. 10(b). To consider diverse silty soils with different SSA values, an upper bound of 70 m²/g and a lower bound of 20 m^2/g are imposed to the scaling relationship while the Hamaker constant and average water density remain unchanged. As such, a band area is produced for the calculated SWR data, and the experimental SWR measurements of four natural silty soils found in the literature (Jackson et al. 1965; Jensen et al. 2015; Lu 2016, 2019b) all reside nicely within the prediction region. These findings reveal a potentially promising future for the application of vapor sorption analysis (VSA) to assess the role of cavitation in soil water drainage because the VSA can provide accurate information about the parameters (i.e., A_H , SSA, and ρ_w^{ave}) necessary for the framework developed in this study.

Practical Implications

Physical Cavitation Sites in Soil

For room temperature, water cavitation can take place at a wide range of water pressures from as low as -186 MPa to as high

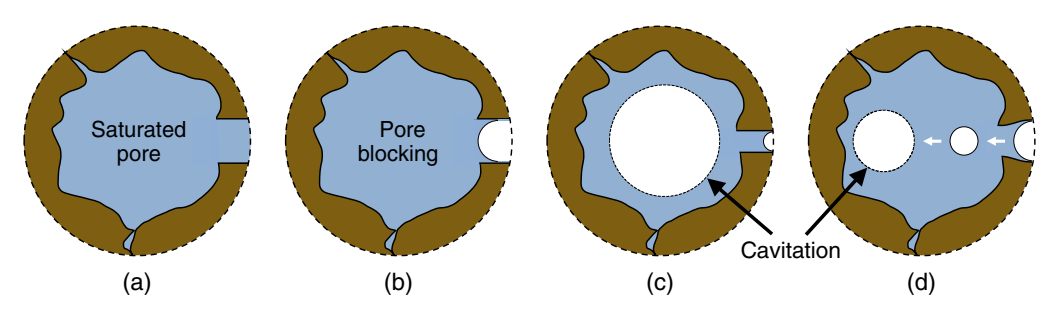


Fig. 11. Idealized models illustrating the mechanisms of water drainage in a large cavity confined by a narrow neck: (a) saturated condition; (b) appearance of pore blocking when the neck diameter D is larger than a critical size D_{crit} ; (c) appearance of cavitation when D is less than D_{crit} ; and (d) intake of air due to the uneven neck diameter.

as -100 kPa, as discussed previously. Although the fundamental mechanisms that dictate the cavitation of soil water are even more complicated due to the SSP, they can still be classified into a few major types based on how the water is drained away from a saturated pore space shown in Fig. 11(a) (e.g., Or and Tuller 2002). This idealized pore geometry for soil or other porous media is well known as the ink-bottle pore model because it is composed of cavity and narrow neck pores. The narrow neck functions as a water plug to prevent the water in the cavity from evaporation during the desaturation process (e.g., Maheshwari et al. 2016).

Generally, the drainage of water in such a confined pore can be in the form of either evaporation or cavitation, mainly depending on the size of the neck width (Thommes et al. 2006; Thommes and Cychosz 2014). If the pore neck width is larger than a certain critical size, the drainage of water in the large cavity will be impeded by the neck, which is known as pore blocking [Fig. 11(b)]. The cavity remains saturated until the capillary water in the neck evaporates. However, when the neck size is smaller than the critical value, the water will evaporate at a lower vapor pressure, causing the cavitation of water in the large pore prior to the water evaporation in the neck [Fig. 11(c)]. This process, or evaporation-induced cavitation, is experimentally captured in nanopores of silicon material (Duan et al. 2012). Because water in the confined pore space transforms from liquid into the same volume of vapor and a density ratio of liquid to vapor is equal to 5×10^4 , to conserve mass the majority of pore water needs to be physically removed via the air-water interface in the neck, and such phenomenon can be referred to as the cavitation-induced evaporation (Cychosz et al. 2017). Therefore, both pore blocking and cavitation can cause delay of pore evaporation and hence hysteresis on the adsorption-desorption cycle.

Nevertheless, neither pore blocking nor cavitation discussed previously considers a very common situation in unsaturated soils, which is the preexisting gas bubble entrapped in the large pore. In a natural environment, the entrapped gas bubbles are unlikely to vanish, owning to the thermodynamic conditions in the crevices (Or and Tuller 2003). Considering a desorption isotherm for a silty soil as the example, the confined cavity seeded with a bubble can be drained gradually as the bubble grows quasi-statically during a continuous decrease in relative humidity (RH). Once the critical liquid pressure is reached, the entire pore space is then emptied by the indefinite growth of bubble [Fig. 11(c)]. This process is usually not restricted by neck width because the matric suction threshold determined for the onset of cavitation only ranges from 100 to 400 kPa. This suction range corresponds to the RH > 0.99 according to Kelvin's equation (e.g., Lu and Likos 2004), in which regime the capillary effect dominates the matric suction.

Another possible way to introduce bubble as the cavitation nucleus is from the pore neck entrance. For soil under the natural drainage condition like a water table decline, a variety of pore sizes should be expected and the PSD will be far from the idealized bimodal distribution displayed in Fig. 11(a). The study of water behavior in a nanofluidic channel manifests that air can enter into the pore space during desorption if the neck width varies, as demonstrated experimentally by Duan et al. (2012) and illustrated in Fig. 11(d). Photos taken by a high-speed camera (Duan et al. 2012) reveal that the intake air forms the seed bubble that rapidly moves toward the center of the channel and initiates an outward growth. As such, a sudden drop on the desorption path, which is often considered as the signature of cavitation occurrence in the nitrogen sorption isotherm (e.g., Coasne et al. 2013), is rarely observed for water vapor sorption isotherms obtained from soil because of the drainage mechanism shown in Fig. 11(d). In soil, water in the cavity gradually cavitates over the range of RH (0.3-0.99) during the desorption process as long as the air bubble makes its way into the pore neck. On the contrary, the pore blocking [Fig. 11(b)] or cavitation [Fig. 11(c)] is almost always observed on the nitrogen isotherm measured at 77 K (Coasne et al. 2013). This is because a step of outgassing by vacuum pumping prior to isotherm measurement is required to remove all physically adsorbed materials from the sample surface before the experiment (Thommes et al. 2006; Thommes and Cychosz 2014), leading to a very different testing environment than that of the water vapor adsorption/desorption. For the nitrogen adsorption at 77 K, the critical neck width is about 6 nm, and the neck length is also found to have an effect on the evaporation process (Zeng et al. 2014).

Implication of Metastable Cavitation in the Limitation of Axis Translation Technique

AT is arguably the most widely used laboratory technique for controlling matric suction in unsaturated soil testing. Two assumptions are inherently involved in AT: cavitation is not important in SWR, and matric suction can be defined only as the difference between pore air pressure p_a and pore water pressure p_w , i.e.

$$-\psi_m = p_a - p_w \tag{28}$$

This definition of matric suction has been recently shown to be incomplete and is a special case of the general matric potential Eq. (8), because Eq. (28) overlooks adsorptive potential and only defines capillary potential (Lu and Zhang 2019). As demonstrated experimentally (Lu 2019b) and here through the new cavitation framework in the preceding sections, cavitation of soil likely occurs during the AT test, particularly crevices on particle surfaces in silty soils. The current prediction here is based on the simple assumption that crevice size and morphology on particle surfaces follow a uniform distribution. Further detailed studies on the likely

distributions of crevice size and morphology utilizing the presented cavitation framework will provide more definite answers to the importance of cavitation in soil, and consequently the limitations of AT for laboratory SWR curve measurements.

Conclusions

Water cavitation has been considered as one of the mechanisms important for soil water retention, yet it has not been explicitly considered in most SWR curve models due to the lack of quantitative framework for cavitation of soil water. This work develops a framework for cavitation of soil water. Critical assessments of the classical cavitation nucleation theories in fluid and porous media for their applicability in soil under the existence of soil sorptive potential are provided.

According to the classical nucleation theories, liquid water can be in a metastable state when stretched below its saturated vapor pressure at a given temperature. To trigger the phase transition (i.e., cavitation) via either homogeneous (e.g., CNT) or heterogeneous nucleation, the average energy of thermal fluctuation of water molecules needs to surmount an energy barrier so that a large enough vapor bubble can form inside the liquid body and its further growth in size is energetically favorable. Homogeneous nucleation theories generally predict very low cavitation pressures from -100 to -200 MPa at room temperature, while the energy barrier for heterogeneous nucleation is highly dependent on the surface contact angle. Although similar properties to homogeneous nucleation can be expected for the hydrophilic surface, the energy barrier may theoretically disappear when nucleating on a perfectly nonwetting surface.

The phase transition behavior of soil water is remarkably different than that of free water and thus the local intermolecular pressure, instead of the bulk water pressure within the pore space, should be considered. The SSP increases the water pressure in nanopores as well as near the soil particle surface by acting adsorptive forces on soil water, which reduces the nucleation events and suppresses the water cavitation in the high matric suction regions (e.g., >100 MPa). It is concluded that both homogeneous nucleation and heterogeneous nucleation are unlikely to occur in soil water or smooth particle surfaces because SSP elevates intermolecular water pressure and effectively suppresses water cavitation.

Entrapped gas cavitation, occurring in crevices greater than nanometers on or near soil particle surfaces, can cause water cavitation in soil. The proposed framework for predicting water cavitation pressure with such mechanism employs a crevice model [Eqs. (15)–(19)] for entrapped gas nucleation and Blake threshold [Eqs. (21)–(24)] for bubble evolution within capillary pore water at the metastable state. The framework is validated against experimental data obtained for four silty soils. The calculated cavitation pressure, together with SSP, is used to predict the SWR curve of the soil. The predicted SWR curve closely follows the measured SWR curve data under natural conditions, confirming the validity of the framework, and the limitation of the AT method for measuring the SWR curve.

Preexisting gas acting as the nucleus can cause the cavitation of soil water in micrometer to submicrometer pores $(10^{-7}-10^{-5} \text{ m})$, especially for silty soils. The proposed framework predicts the cavitation regime within the matric suction range between 100 and 2,200 kPa, and the calculated SWR regime closely encloses the experiment data obtained from four silty soils using the DP method. The obvious discrepancy between the proposed framework (as well as the DP) and the AT technique further confirms the fact that the AT may prevent cavitation and thus fails to reflect the actual field

conditions. Therefore, cavitation could be a significant mechanism for water drainage in the capillary-dominant soil and should be quantitatively characterized in SWR curve models.

Data Availability Statement

All data, models, and code generated or used during the study appear in the published article.

Acknowledgments

This research is supported by the US National Science Foundation (NSF CMMI-1902045 and CMMI-1902008).

References

- Akin, I. D., and W. J. Likos. 2017. "Implications of surface hydration and capillary condensation for strength and stiffness of compacted clay." *J. Eng. Mech.* 143 (8): 04017054. https://doi.org/10.1061/(ASCE)EM .1943-7889.0001265.
- Akin, I. D., and W. J. Likos. 2020. "Suction stress of clay over a wide range of saturation." *Geotech. Geol. Eng.* 38 (1): 283–296. https://doi.org/10 .1007/s10706-019-01016-7.
- Atchley, A. A. 1989. "The Blake threshold of a cavitation nucleus having a radius-dependent surface tension." *J. Acoust. Soc. Am.* 85 (1): 152–157. https://doi.org/10.1121/1.397724.
- Atchley, A. A., and A. Prosperetti. 1989. "The crevice model of bubble nucleation." J. Acoust. Soc. Am. 86 (3): 1065–1084. https://doi.org/10 .1121/1.398098.
- Baker, R., and S. Frydman. 2009. "Unsaturated soil mechanics: Critical review of physical foundations." *Eng. Geol.* 106 (1): 26–39. https://doi.org/10.1016/j.enggeo.2009.02.010.
- Belova, V., D. A. Gorin, D. G. Shchukin, and H. Möhwald. 2010. "Selective ultrasonic cavitation on patterned hydrophobic surfaces." *Angew. Chem. Int. Ed.* 49 (39): 7129–7133. https://doi.org/10.1002/anie 201002069
- Belova, V., D. A. Gorin, D. G. Shchukin, and H. Möhwald. 2011. "Controlled effect of ultrasonic cavitation on hydrophobic/hydrophilic surfaces." ACS Appl. Mater. Interfaces 3 (2): 417–425. https://doi.org/10.1021/am101006x.
- Bittelli, M., and M. Flury. 2009. "Errors in water retention curves determined with pressure plates." *Soil Sci. Soc. Am. J.* 73 (5): 1453–1460. https://doi.org/10.2136/sssaj2008.0082.
- Blake, F. G. 1949. The onset of cavitation in liquids. Technical Memorandum No. 12. Cambridge, MA: Acoustics Research Laboratory, Harvard Univ
- Blander, M., and J. L. Katz. 1975. "Bubble nucleation in liquids." *AIChE J.* 21 (5): 833–848. https://doi.org/10.1002/aic.690210502.
- Brennen, C. E. 2013. *Cavitation and bubble dynamics*. Cambridge, UK: Cambridge University Press.
- Briggs, L. J. 1950. "Limiting negative pressure of water." *J. Appl. Phys.* 21 (7): 721–722. https://doi.org/10.1063/1.1699741.
- Caupin, F. 2005. "Liquid-vapor interface, cavitation, and the phase diagram of water." *Phys. Rev. E* 71 (5): 051605. https://doi.org/10.1103/PhysRevE.71.051605.
- Caupin, F., A. Arvengas, K. Davitt, M. E. M. Azouzi, K. I. Shmulovich, C. Ramboz, D. A. Sessoms, and A. D. Stroock. 2012. "Exploring water and other liquids at negative pressure." *J. Phys.: Condens. Matter* 24 (28): 284110. https://doi.org/10.1088/0953-8984/24/28/284110.
- Caupin, F., and E. Herbert. 2006. "Cavitation in water: A review." C.R. Phys. 7 (9): 1000–1017. https://doi.org/10.1016/j.crhy.2006.10.015.
- Chahal, R. S., and R. N. Yong. 1965. "Validity of the soil water characteristics determined with the pressurized apparatus." *Soil Sci.* 99 (2): 98–103. https://doi.org/10.1097/00010694-196502000-00006.
- Coasne, B., A. Galarneau, R. J. M. Pellenq, and F. Di Renzo. 2013. "Adsorption, intrusion and freezing in porous silica: The view from

- the nanoscale." *Chem. Soc. Rev.* 42 (9): 4141–4171. https://doi.org/10 .1039/c2cs35384a.
- Cychosz, K. A., R. Guillet-Nicolas, J. García-Martínez, and M. Thommes. 2017. "Recent advances in the textural characterization of hierarchically structured nanoporous materials." *Chem. Soc. Rev.* 46 (2): 389–414. https://doi.org/10.1039/C6CS00391E.
- Debenedetti, P. G. 1996. *Metastable liquids: Concepts and principles*. Princeton, NJ: Princeton University Press.
- Debenedetti, P. G., and H. Reiss. 1998. "Reversible work of formation of an embryo of a new phase within a uniform macroscopic mother phase." *J. Chem. Phys.* 108 (13): 5498–5505. https://doi.org/10.1063/1.475938.
- Derjaguin, B. V., N. V. Churaev, and V. M. Muller. 1987. *Surface forces*. New York: Plenum Publishing.
- Duan, C., R. Karnik, M.-C. Lu, and A. Majumdar. 2012. "Evaporation-induced cavitation in nanofluidic channels." *Proc. Natl. Acad. Sci.* 109 (10): 3688–3693. https://doi.org/10.1073/pnas.1014075109.
- Factorovich, M. H., E. Gonzalez Solveyra, V. Molinero, and D. A. Scherlis. 2014. "Sorption isotherms of water in nanopores: Relationship between hydropohobicity, adsorption pressure, and hysteresis." *J. Phys. Chem. C* 118 (29): 16290–16300. https://doi.org/10.1021/jp5000396.
- Favvas, E. P., and A. C. Mitropoulos. 2008. "What is spinodal decomposition?" J. Eng. Sci. Technol. Rev. 1 (1): 25–27. https://doi.org/10.25103/jestr.011.05.
- Frydman, S., and R. Baker. 2009. "Theoretical soil-water characteristic curves based on adsorption, cavitation, and a double porosity model." *Int. J. Geomech.* 9 (6): 250–257. https://doi.org/10.1061/(ASCE)1532 -3641(2009)9:6(250).
- Giacomello, A., and R. Roth. 2020. "Bubble formation in nanopores: A matter of hydrophobicity, geometry, and size." *Adv. Phys.: X* 5 (1): 1817780. https://doi.org/10.1080/23746149.2020.1817780.
- Greenspan, M., and C. E. Tschiegg. 1967. "Radiation-induced acoustic cavitation: Apparatus and some results." J. Res. Nat. Bur. Stand. 71C (4): 299–312.
- Groß, T. F., and P. F. Pelz. 2017. "Diffusion-driven nucleation from surface nuclei in hydrodynamic cavitation." *J. Fluid Mech.* 830 (Nov): 138–164. https://doi.org/10.1017/jfm.2017.587.
- Gunther, L. 2003. "A comprehensive treatment of classical nucleation in a supercooled or superheated fluid." Am. J. Phys. 71 (4): 351–357. https:// doi.org/10.1119/1.1528914.
- Herbert, E., S. Balibar, and F. Caupin. 2006. "Cavitation pressure in water." Phys. Rev. E 74 (4): 041603. https://doi.org/10.1103/PhysRevE.74 041603
- Hilf, J. W. 1956. An investigation of pore water pressure in compacted cohesive soils. Boulder, CO: Univ. of Colorado at Boulder.
- Hillel, D. 1998. Environmental soil physics. San Diego: Academic Press. Iwamatsu, M., and K. Horii. 1996. "Capillary condensation and adhesion of two wetter surfaces." J. Colloid Interface Sci. 182 (2): 400–406. https:// doi.org/10.1006/jcis.1996.0480.
- Jackson, R. D., R. J. Reginato, and C. H. M. Van Bavel. 1965. "Comparison of measured and calculated hydraulic conductivities of unsaturated soils." Water Resour. Res. 1 (3): 375–380. https://doi.org/10.1029 /WR001i003p00375.
- Jensen, D. K., M. Tuller, L. W. de Jonge, E. Arthur, and P. Moldrup. 2015. "A new two-stage approach to predicting the soil water characteristic from saturation to oven-dryness." *J. Hydrol.* 521 (Feb): 498–507. https://doi.org/10.1016/j.jhydrol.2014.12.018.
- Karthika, S., T. K. Radhakrishnan, and P. Kalaichelvi. 2016. "A review of classical and nonclassical nucleation theories." *Cryst. Growth Des.* 16 (11): 6663–6681. https://doi.org/10.1021/acs.cgd.6b00794.
- Lienhard, J. H., N. Shamsundar, and P. O. Biney. 1986. "Spinodal lines and equations of state: A review." *Nucl. Eng. Des.* 95 (Aug): 297–314. https://doi.org/10.1016/0029-5493(86)90056-7.
- Liu, Z., F. Liu, F. Ma, M. Wang, X. Bai, Y. Zheng, H. Yin, and G. Zhang. 2016. "Collapsibility, composition, and microstructure of loess in China." Can. Geotech. J. 53 (4): 673–686. https://doi.org/10.1139/cgj -2015-0285.
- Lu, N. 2016. "Generalized soil water retention equation for adsorption and capillarity." J. Geotech. Geoenviron. Eng. 142 (10): 04016051. https:// doi.org/10.1061/(ASCE)GT.1943-5606.0001524.

- Lu, N. 2019a. "Linking soil water adsorption to geotechnical engineering properties." In *Geotechnical fundamentals for addressing new world* challenges, edited by N. Lu and J. K. Mitchell, 93–139. Cham, Switzerland: Springer.
- Lu, N. 2019b. "Revisiting axis translation for unsaturated soil testing." J. Geotech. Geoenviron. Eng. 145 (7): 02819001. https://doi.org/10.1061/(ASCE)GT.1943-5606.0002055.
- Lu, N. 2020. "Unsaturated soil mechanics: Fundamental challenges, break-throughs, and opportunities." J. Geotech. Geoenviron. Eng. 146 (5): 02520001. https://doi.org/10.1061/(ASCE)GT.1943-5606.0002233.
- Lu, N., M. T. Anderson, W. J. Likos, and G. W. Mustoe. 2008. "A discrete element model for kaolinite aggregate formation during sedimentation." *Int. J. Numer. Anal. Methods Geomech.* 32 (8): 965–980. https://doi.org/10.1002/nag.656.
- Lu, N., and M. Khorshidi. 2015. "Mechanisms for soil-water retention and hysteresis at high suction range." J. Geotech. Geoenviron. Eng. 141 (8): 04015032. https://doi.org/10.1061/(ASCE)GT.1943-5606.0001325.
- Lu, N., and W. J. Likos. 2004. Unsaturated soil mechanics. New York: Wiley.
- Lu, N., and C. Zhang. 2019. "Soil sorptive potential: Concept, theory, and verification." J. Geotech. Geoenviron. Eng. 145 (4): 04019006. https:// doi.org/10.1061/(ASCE)GT.1943-5606.0002025.
- Maheshwari, P., D. Dutta, T. Muthulakshmi, B. Chakraborty, N. Raje, and P. K. Pujari. 2016. "Desorption of water from hydrophilic MCM-41 mesopores: Positron annihilation, FTIR and MD simulation studies." *J. Phys.: Condens. Matter* 29 (5): 055003. https://doi.org/10.1088/1361 -648X/29/5/055003.
- Marinho, F. A. M., W. A. Take, and A. Tarantino. 2008. "Measurement of matric suction using tensiometric and axis translation techniques." *Geotech. Geol. Eng.* 26 (6): 615. https://doi.org/10.1007/s10706-008 -9201-8.
- Maris, H., and S. Balibar. 2000. "Negative pressures and cavitation in liquid helium." *Phys. Today* 53 (2): 29–34. https://doi.org/10.1063/1.882962.
- Maruyama, I., J. Rymeš, M. Vandamme, and B. Coasne. 2018. "Cavitation of water in hardened cement paste under short-term desorption measurements." *Mater. Struct.* 51 (6): 159. https://doi.org/10.1617/s11527 -018-1285-x.
- Mitchell, J. K. 1962. "Components of pore water pressure and their engineering significance." In *Proc.*, 9th National Conf. on Clays and Clay Minerals, 162–184. West Lafayette, IN: Pergamon Press.
- Nitao, J. J., and J. Bear. 1996. "Potentials and their role in transport in porous media." *Water Resour. Res.* 32 (2): 225–250. https://doi.org/10.1029/95WR02715.
- Or, D., and M. Tuller. 2002. "Cavitation during desaturation of porous media under tension." *Water Resour. Res.* 38 (5): 14–19. https://doi.org/10.1029/2001WR000282.
- Or, D., and M. Tuller. 2003. "Reply to comment by N. Kartal Toker, John T. Germaine, and Patricia J. Culligan on 'Cavitation during desaturation of porous media under tension." *Water Resour. Res.* 39 (11): 1306. https://doi.org/10.1029/2003WR002492.
- Pettersen, M. S., S. Balibar, and H. J. Maris. 1994. "Experimental investigation of cavitation in superfluid ⁴He." *Phys. Rev. B* 49 (17): 12062–12070. https://doi.org/10.1103/PhysRevB.49.12062.
- Revil, A., and N. Lu. 2013. "Unified water isotherms for clayey porous materials." Water Resour. Res. 49 (9): 5685–5699. https://doi.org/10 .1002/wrcr.20426.
- Shamsundar, N., and J. H. Lienhard. 1993. "Equations of state and spinodal lines—A review." *Nucl. Eng. Des.* 141 (1): 269–287. https://doi.org/10 .1016/0029-5493(93)90106-J.
- Silbey, R. J., R. A. Alberty, and M. G. Bawendi. 2004. *Physical chemistry*. New York: Wiley.
- Thommes, M., and K. A. Cychosz. 2014. "Physical adsorption characterization of nanoporous materials: Progress and challenges." *Adsorption* 20 (2): 233–250. https://doi.org/10.1007/s10450-014-9606-z.
- Thommes, M., B. Smarsly, M. Groenewolt, P. I. Ravikovitch, and A. V. Neimark. 2006. "Adsorption hysteresis of nitrogen and argon in pore networks and characterization of novel micro- and mesoporous silicas." *Langmuir* 22 (2): 756–764. https://doi.org/10.1021/la051686h.
- Toker, N. K., J. T. Germaine, and P. J. Culligan. 2003. "Comment on 'Cavitation during desaturation of porous media under tension' by

- Dani Or and Markus Tuller." *Water Resour. Res.* 39 (11): 1305. https://doi.org/10.1029/2002WR001834.
- Tuller, M., and D. Or. 2005. "Water films and scaling of soil characteristic curves at low water contents." Water Resour. Res. 41 (9): W09403. https://doi.org/10.1029/2005WR004142.
- Tuller, M., D. Or, and L. M. Dudley. 1999. "Adsorption and capillary condensation in porous media: Liquid retention and interfacial configurations in angular pores." Water Resour. Res. 35 (7): 1949–1964. https://doi.org/10.1029/1999WR900098.
- von Fay, K. F. 1985. Review of negative pore pressure: Its measurement, and testing of the CRL apparatus. Denver: Geotechnical Branch, Division of Research and Laboratory Services, Engineering and Research Center.
- Wagner, W., and A. Pruß. 2002. "The IAPWS formulation 1995 for the thermodynamic properties of ordinary water substance for general and scientific use." J. Phys. Chem. Ref. Data 31 (2): 387–535. https:// doi.org/10.1063/1.1461829.

- Zeng, Y., C. Fan, D. D. Do, and D. Nicholson. 2014. "Evaporation from an ink-bottle pore: Mechanisms of adsorption and desorption." *Ind. Eng. Chem. Res.* 53 (40): 15467–15474. https://doi.org/10.1021/ie500215x.
- Zhang, C., and N. Lu. 2018. "What is the range of soil water density? Critical reviews with a unified model." Rev. Geophys. 56 (3): 532–562. https://doi.org/10.1029/2018RG000597.
- Zhang, C., and N. Lu. 2020. "Soil sorptive potential: Its determination and predicting soil water density." *J. Geotech. Geoenviron. Eng.* 146 (1): 04019118. https://doi.org/10.1061/(ASCE)GT.1943-5606.0002188.
- Zheng, Q., D. J. Durben, G. H. Wolf, and C. A. Angell. 1991. "Liquids at large negative pressures: Water at the homogeneous nucleation limit." *Science* 254 (5033): 829–832. https://doi.org/10.1126/science.254 .5033.829.
- Zheng, Y., and A. Zaoui. 2017. "Wetting and nanodroplet contact angle of the clay 2:1 surface: The case of Na-montmorillonite (001)." *Appl. Surf. Sci.* 396 (Feb): 717–722. https://doi.org/10.1016/j.apsusc.2016.11.015.